Structure and composition of sputter-deposited nickel-tungsten oxide films

S. V. Green[1*], A. Kuzmin[2], J. Purans[2], C. G. Granqvist[1], G. A. Niklasson[1]

1. Department of Engineering Sciences, The Ångström Laboratory, Uppsala University, P.O. Box 534, SE-751 21 Uppsala, Sweden

2. Institute of Solid State Physics, University of Latvia, 8 Kengaraga Street, Riga, Latvia

*Corresponding author: tel: +46 18 471 3129, fax: +46 18 471 3270,

email: sara.green@angstrom.uu.se

Abstract

Films of mixed nickel-tungsten oxide, denoted Ni_xW_{1-x} oxide, were prepared by reactive DC magnetron co-sputtering from metallic targets and were characterized by Rutherford backscattering spectrometry, X-ray photoelectron spectroscopy, X-ray diffractometry and Raman spectroscopy. A consistent picture of the structure and composition emerged, and at $x < 0.50$ the films comprised a mixture of amorphous WO_3 and nanosized $NiWO_4$, at $x = 0.50$ the nanosized $NiWO_4$ phase was dominating, and at $x > 0.50$ the films contained nanosized NiO and $NiWO_4$, and possibly also WO_3.

Keywords

Tungsten oxide, Nickel oxide, X-ray photoelectron spectroscopy, Rutherford backscattering, X-ray diffraction, Raman spectroscopy

1. Introduction

Films of tungsten oxide and nickel oxide have many applications, such as in electrochromic devices, gas sensors and photocatalytic surfaces [1,2]. Mixed nickel-tungsten oxide films, denoted Ni_xW_{1-x} oxide, may have properties that are superior to those of the two components and were investigated in this work. The main objective is to elucidate the structural evolution of the phases that emerge for $0 < x < 1$.

Our specific interest is connected with the electrochromic properties of the Ni_xW_{1-x} oxide system. Electrochromic materials change their optical properties when a potential is applied so that electrical charge is inserted or extracted, and both tungsten oxide and nickel oxide are widely used materials with excellent and complementary electrochromic properties [1-3]. The electrochromic effect ensues from electron transitions between different atomic states. For tungsten oxide, electron transitions between W^{5+} and W^{6+} cause absorption which sets in progressively as the W^{5+} content is increased. Nickel oxides with Ni^{2+} are transparent, which is the case for NiO and/or $Ni(OH)_2$, whereas oxides with Ni^{3+} are absorbing and this is so for NiOOH and/or Ni_2O_3.

Mixed oxide thin films can have improved electrochromic properties, as has been known for many years [2,4-7], and at least one study has been made on thin film electrochromic tungsten oxide containing nickel, showing that the additive had beneficial effects led to faster response times for the optical modulation, lower power consumption and good stability [8]. There is also some prior work by Kuzmin *et al.* on thin films of nickel tungstate, $NiWO_4$, with foci on local atomic structure and electrochromic properties [9,10].

The phase diagram for the bulk NiO-WO_3 system forms a suitable point of departure for discussing thin films of this material. The system does not form solid solutions and the only compound $NiWO_4$ melts incongruently at 1420ºC and forms a eutectic with WO_3 at 73 mol % WO_3 and 1245ºC [11]. The crystalline phases present after solidification of melts yields are comprised of NiO + $NiWO_4$ and $NiWO_4$ + WO_3 in the composition range below and above 50 mol % WO_3, respectively. These results may provide guide lines for structural evolutions, but films of Ni_xW_{1-x} oxide can sustain metastable phases so that structural and compositional characterizations are essential in order to develop a fundamental understanding of their properties, notably for the electrochromic performance. To that end we studied sputter deposited Ni_xW_{1-x} oxide films with several different techniques, specifically being Rutherford backscattering spectrometry (RBS), X-ray photoelectron spectroscopy (XPS), X-ray diffractometry (XRD), and Raman spectroscopy (RS).

The present work forms part of a larger investigation of electrochromic films of Ni_xW_{1-x} oxide. As a starting point for this investigation, we reported recently on the electrochromism of pure tungsten oxide and nickel oxide in various electrolytes [12].

2. Sample preparation and characterization techniques

Mixed nickel-tungsten oxide thin films were made by reactive DC magnetron co-sputtering from separate 5-cm-diameter targets of pure tungsten and nickel in a versatile deposition system based on a Balzer UTT 400 unit. Depositions took place in a gas mixture with an O_2/Ar mass flow ratio of 0.15 and a working pressure of ~30 mTorr. The target-substrate separation was ~13 cm. The total discharge power, $P_W + P_{Ni}$, was set to 230 W. The power to the targets was varied in order to obtain Ni_xW_{1-x} oxide thin films with different magnitudes of x. Some samples were deposited onto unheated 5 x 5 cm^2 glass plates precoated with

transparent and electron conductive In_2O_3:Sn (ITO) in order to allow electrochemical measurements for subsequent investigation of the electrochromic properties. The XPS measurements used small pieces of such films. XRD, RBS and RS measurements were made on films deposited onto Si, C and pure glass, respectively. Some samples on silicon substrates were post-treated at 800ºC for 6.5 h in air in order to induce crystallization. Film thicknesses, as measured by an Alpha step profilometer, were 200 to 300 nm except for some RS samples that were as thick as 1 μm in order to ensure good Raman signals.

RBS gave information on composition and density for the whole film-substrate system when data were fitted to a model by use of the SIMNRA code [13]. The spectra reveal what kind of atom is detected (by peak position), atomic concentration (by relative peak height), and thickness in atoms/cm^2 (by peak width). These measurements were carried out at the Uppsala Tandem Laboratory using 2 MeV ^{4}He ions backscattered at an angle of 172º.

XPS measurements were performed with a PHI Quantum 2000 Scanning ESCA Microprobe operating with monochromated AlK_α radiation (1486 eV), pass energy of 46.95 eV and step size of 0.2 eV/s. Energy calibration was done by setting the binding energy of C1s to 284.5 eV. Spectra were analysed using the Multipak program [14] and the magnitude of x was obtained from integration over the W4f and Ni2p peaks.

XRD information was recorded on a Siemens D5000 diffractometer operating with CuK_α radiation at a wavelength of 1.54 Å. The detector was a parallel plate collimator with an acceptance angle of 0.4º. During measurements the incoming beam was fixed at an angle of 1º, and the detector angle was scanned with 2 s/step for increments of 0.05º. Structure, phase

composition and orientation of the planes were inferred by comparing experimental spectra with the JCPDS database.

RS data were taken at room temperature (20°C) by use of a confocal microscope with a "Nanofinder-S" (SOLAR TII, Ltd.) spectrometer [15]. The measurements were performed through a Nikon CF Plan Apo 100× (NA = 0.95) optical objective. The Raman spectra were excited with a He-Cd laser (441.6 nm, 50mW cw power) and dispersed by a 600 grooves/mm diffraction grating mounted in a 520 mm focal length monochromator. To exclude possible sample heating, the laser power at the sample was regulated by a variable neutral-density filter (optical density from zero to 3.1). A Peltier-cooled back-thinned CCD camera (ProScan HS-101H, 1024x58 pixels) was used as detector. The elastic laser light component was eliminated by an edge filter (Omega, 441.6AELP-GP).

3. Results and discussion

3.1 Composition found by RBS and XPS

The composition dependence of the Ni_xW_{1-x} oxide thin films on the sputter power ratio P_{Ni}/P_W was readily inferred from RBS and XPS as shown in figure 1. The values from the two sets of measurements were in good agreement. The figure also illustrates whether the samples were visually transparent or not. The colour of the dark films was brownish. The density, found by RBS, lay close to that of W oxide films, *i.e.* in the 5 to 6 g/cm^3 range [2,12].

3.2 W 4f, Ni 2p and O 1s binding energies analyzed by XPS

XPS is a surface sensitive technique whose depth sensitivity is limited by the mean-free path of the escaping electron to about 10 to 100 Å. A rigorous treatment of the XPS spectra in transition metal oxides requires an account for many-body charge-transfer effects, which are

responsible for a characteristic splitting of the 2p spectra of transition metal compounds [16]. In the present work, we will limit our analysis of the Ni 2p, W 4f and O 1s XPS spectra to the estimation of binding energies and peak intensities, which will be used to evaluate the oxidation state of metal ions and the film compositions. A comparison with known XPS data will be given for several reference compounds.

3.2.1 W 4f

In pure tungsten oxide, *i.e.* $W^{6+}O_3$, the W $4f_{7/2}$ and W $4f_{5/2}$ peaks lie at 35.6 and 37.7 eV, respectively [17,18]. The positions of the two peaks for W^{5+} are located at lower binding energies, specifically at 34.9 and 37.1 eV [18]. Even smaller binding energies, at 33.5 and 35.8 eV, are expected for W^{4+} [18]. The binding energy for W $4f_{7/2}$ in $NiWO_4$ has been found to lie at 35.4 [17] and 35.2 eV [19], *i.e.* close to that of W^{6+}.

Figure 2 shows that the W 4f spectra in our films consist of well-resolved spin orbit split doublet peaks corresponding to W $4f_{7/2}$ and W $4f_{5/2}$ states. For the pure W oxide film the locations of the two peaks suggest a W^{6+} state. No change, as compared to the case of pure transparent W oxide, was found for films with Ni contents up to $x \approx 0.20$. Upon addition of up to $x = 0.5$, the binding energies of W $4f_{7/2}$ and W $4f_{5/2}$ states decreased slightly and some peak broadening was observed. As even more Ni was added, a film with $x = 0.75$ became dark in colour and the double peak changed to lower binding energies, as shown in figure 2. This peak shift is due to the presence of reduced tungsten ions W^{5+} [2,18]. For $x = 0.50$ the peak is displaced to a binding energy close to that of $NiWO_4$, but the shift for the dark $Ni_{0.75}W_{0.25}$ oxide could also be due to the presence of W^{5+}. Also the broadening of the peak for $Ni_{0.50}W_{0.50}$ oxide could be associated with W^{5+}.

3.2.2. Ni 2p

For nickel oxides the Ni 2p spectra contain multiple peaks at binding energies between about 852 and 870 eV, including the main peak and satellites [20-22]. According to theory for the XPS technique [23-25], these peaks have been interpreted as due to final state effects caused by charge transfer from oxygen to nickel. The Ni $2p_{3/2}$ XPS spectra in $Ni(OH)_2$ and NiOOH [21] have more broadened shapes than in NiO, and the first peak for NiOOH is shifted to larger binding energies thereby reflecting the presence of Ni^{3+}. As mentioned, the Ni 2p spectra are often complex and contain multiple peaks, and it is difficult to assign specific binding energies to the Ni^{2+} and Ni^{3+} states. For example, a recent work put the main peaks for NiO, $Ni(OH)_2$ and NiOOH at 854.7, 855.3 and 855.8 eV, respectively [21]. The main peak due to Ni $2p_{3/2}$ in $NiWO_4$ was reported to lie at 857.7 [17], 857.5 [19] and 856.2 eV [26].

Figure 3 presents XPS spectra for the Ni $2p_{3/2}$ peak. They consist of two broad bands located at 853 to 858 eV and 860 to 866 eV. For $x \leq 0.5$ the positions of the main peak and of the satellite are found at about 856.5 and 863 eV, respectively: these values are close to the binding energy of nickel in $NiWO_4$. The main peak is progressively shifted to lower binding energies for higher nickel content, *i.e.* for $x > 0.5$. At $x = 0.75$ the binding energy of the main peak is decreased by about 1 eV, down to ~855.5 eV. This decrease can be explained by the appearance of a NiO phase in films with $x > 0.5$. However one cannot exclude the presence of NiOOH, since the sample has a darkish brown colour that indicates the presence of some Ni^{3+}, which possibly is responsible for the asymmetry of the XPS peaks.

3.2.3. O 1s

The O 1s binding energy of NiOOH is 531.7 eV [27], while the corresponding energies are 529.6, 531.3 and 531.8 eV for NiO, $Ni(OH)_2$ and Ni_2O_3, respectively [17]. The O 1s binding energy for crystalline $NiWO_4$ lies at 531.5 eV [19] and for WO_3 at 530.6 eV [17].

Figure 4 shows the O 1s peak for pure W oxide and mixed Ni_xW_{1-x} oxide films with different amounts of Ni. The peak at 530.8 eV for pure WO_3 is in close agreement with literature data [17,19,28,29]. An addition of Ni makes the peak widen and shift. It has been shown [30] that the O 1s peak in W oxide is not affected by stoichiometry, *i.e.* the observed changes of the peak should be solely the result of the presence of another phase, caused by nickel ions. A small peak shift towards higher energies can be seen for $x = 0.19$, which could indicate that $NiWO_4$ and/or some Ni oxide phase, probably $Ni(OH)_2$, with higher binding energy is present. For $x = 0.5$ the O 1s peak shifts to 530.4 eV, indicating the presence of nanosized $NiWO_4$. It is expected that a local structure relaxation in nano-$NiWO_4$ will slightly decrease the O 1s binding energy compared to that of crystalline $NiWO_4$. Moreover the phases with larger O 1s binding energies, such as $Ni(OH)_2$, NiOOH and Ni_2O_3, could contribute to the high-energy tail. The larger shift towards lower binding energies, seen for Ni-rich films with $x \geq 0.50$, can be related to the appearance of a nickel oxide phase in which oxygen atoms have lower binding energy. The colour of the film with $x = 0.75$ film and the broadening of the peak towards higher binding energies could also indicate that some Ni^{3+}- containing phase is present.

3.3 Structures determined by XRD

As-deposited pure W oxide and mixed Ni_xW_{1-x} oxide films were found to be X-ray amorphous up to $x = 0.75$. They become crystalline upon high-temperature treatment at 800ºC.

Figure 5 shows results for annealed pure W oxide and mixed Ni_xW_{1-x} oxide film with $x = 0.5$. Both samples have a monoclinic structure and the peaks agree with literature data for WO_3 [31] and $NiWO_4$ [32], respectively. Figure 6 shows results for an as-deposited polycrystalline Ni oxide film and for annealed mixed Ni_xW_{1-x} oxide with $x = 0.75$. The latter film consists primarily of a cubic rock-salt NiO phase [33], but there is some evidence, shown by the peaks marked with asterisks, that $NiWO_4$ is present: this assignment can be made by comparison with the data in figure 5. Our XRD results on annealed thin films are in full agreement with the phase diagram of the bulk system NiO-WO_3 system [11].

3.4 Lattice dynamics probed by Raman spectroscopy

Raman spectroscopy was used to study the local dynamics in Ni_xW_{1-x} oxide films with $x < 0.45$. As-deposited films were X-ray amorphous: however their local structure, and thus the local phonon modes observed by RS, can resemble those of corresponding amorphous/nanocrystalline phases of WO_3, $NiWO_4$ and NiO.

Figure 7 shows typical Raman spectra for thin films of several compositions. The spectra are dominated by two bands, located at about 790 and at 950 to 970 cm^{-1}, whose ratio changes with composition. These two bands are commonly assigned to O-W-O bond stretching and to terminal W=O modes. The Raman signal of the pure tungsten oxide corresponds to that of an

amorphous film [34-36]. Upon an increase of the nickel content, the intensity of the band at 950 cm^{-1} grew and became dominant for $x > 0.2$.

An addition of nickel makes it possible to form local environments similar to those in $NiWO_4$ and NiO. Nickel oxide with rock-salt structure has weak Raman scattering and normally shows a first-order defect-induced broad band at about 500 cm^{-1} [36] or a set of second-order Raman bands with the highest one at ~1100 cm^{-1} [37] neither of which were observed in the spectra in figure 7. Therefore we can exclude the presence of a NiO phase in the mixed films with $x \leq 0.45$. On the other hand $NiWO_4$ has a very strong Raman signal and is easily detected in thin films [15]. This signal is dominated by the 891 cm^{-1} mode, which is typical for tungstates and corresponds to stretching vibration of the W-O pair in the WO_6 group, a so-called "internal" mode [38]. This band is also not present in the spectra in Figure ; this excludes the presence of a crystalline $NiWO_4$ phase, which is consistent with our XRD results.

However, it was found recently [39] that nanosized tungstates, with crystallite sizes below 2 nm, are X-ray amorphous and have a Raman signal very close to that observed in figure 7 for $x = 0.45$, *i.e.* a dominating band located at 970 cm^{-1} and a broad low-intensity band at 790 cm^{-1}. Therefore we conclude that the Ni_xW_{1-x} oxide film with $x = 0.45$ has a nanosized $NiWO_4$ phase, which transfers into crystalline $NiWO_4$ upon annealing at high temperature.

Finally, Raman signals for intermediate compositions with $0 < x < 0.45$ were found to correspond well to a weighted sum of pure amorphous W oxide and nanosized $NiWO_4$ phases, as shown in figure 8. One can utilize this result to estimate the film composition and to compare it with the nominal nickel content. At a nominal $x = 0.12$, for example, the nickel

content in the film, estimated from the decomposition of the Raman signal, is about 0.24 × 0.45 = 0.11.

4. Conclusion

Films of mixed Ni_xW_{1-x} oxide were characterized by four different techniques, specifically being RBS, XPS, XRD and Raman scattering. From RBS analysis we inferred that the density was close to that of pure W oxide films, *i.e.* 5 to 6 g/cm^3. RBS together with XPS gave consistent results for the magnitude of x.

For films with $x < 0.5$, XPS and RS showed clear evidence for a thin film structure of nanosized $NiWO_4$ and WO_y with y close to 3. The two phases are X-ray amorphous. For $x = 0.5$, both XPS and RS show that the main constituent is nanosized $NiWO_4$.

In films with $x > 0.5$, XPS gave evidence for NiO and reduced tungsten ions (W^{5+}). The tail in the O 1s spectrum at energies above 532 eV also indicated the existence of hydrated phases for $x \geq 0.5$ which, however, are difficult to identify. No clear evidence was found for NiOOH and $Ni(OH)_2$, although they are often present in sputter deposited films together with NiO [22]. In addition, the dark brownish colour of films with $x > 0.5$ films indicated the presence of Ni^{3+}. No clear evidence was found for $NiWO_4$ by XPS, but the broadening of both the Ni 2p and O 1s peaks, in addition to the shift in the W 4f peak, could be signs of its presence.

The as-deposited films were X-ray amorphous for $x \leq 0.75$, but XRD on annealed samples showed that the $Ni_{0.5}W_{0.5}$ oxide film forms $NiWO_4$ and that the $Ni_{0.75}W_{0.25}$ oxide film forms a mixture of NiO and $NiWO_4$. These results are in agreement with the phase diagram for NiO-WO_3 [11].

Finally, our analysis has given a consistent picture for the structure of the notoriously difficult Ni_xW_{1-x} oxide thin films, as summarised in table 1. This information is useful for a number of applications including electrochromics (as will be elaborated in a later paper), conductometric gas sensors, photocatalysts, and others.

Acknowledgments

This work was supported by Clear-up (Clean and Resource Efficient Buildings for Real Life) which is an Integrated Project funded by the European Community's Seventh Framework Programme (FP7/2007-2013) under grant agreement number 211948. Additional support was received from the Swedish Research Council for Environment, Agriculture Sciences and Spatial Planning (FORMAS) and by a scholarship from the Anna-Maria Lundin foundation. We are grateful to Jens Jensen for valuable input regarding RBS measurements.

References

[1] G. B. Smith, C. G. Granqvist, Green Nanotechnology: Solutions for Sustainability and Energy in the Built Environment, CRC Press, Boca Raton, FL, USA, 2010, (to be published).

[2] C. G. Granqvist, Handbook of Inorganic Electrochromic Materials, Elsevier, Amsterdam, The Netherlands, 1995.

[3] G. A. Niklasson, C. G. Granqvist, J. Mater. Chem. 17 (2007), 127.

[4] B. W. Faughnan, R. S. Crandall, Appl. Phys. Lett. 31 (1977) 834.

[5] S. Sato, Y. Seino, Trans. Inst. Electr. Commun. Engr. Japan 65-C (1982) 629.

[6] S. Yamada, M. Kitao, Modulation of absorption spectra by the use of mixed films of $Mo_cW_{1-c}O_3$, in Large-Area Chromogenics: Materials and Devices for Transmittance Control, edited by C. M. Lampert, C. G. Granqvist, SPIE–The International Society for Optical Engineering, Bellingham, WA, USA, 1990, pp. 246.

[7] E. Avendaño, A. Azens, G. A. Niklasson, C. G. Granqvist, Sol. Energy Mater. Sol. Cells 84 (2004) 337.

[8] P. K. Shen, J. Syed-Bokhari, A. C. C Tseung, J. Electrochem. Soc. 138 (1991) 2778.

[9] A. Kuzmin, J. Purans, R. Kalendarev, D. Pailharey, Y. Mathey, Electrochim. Acta 46 (2001) 2233.

[10] A. Kuzmin, J. Purans, R. Kalendarev, Ferroelectrics 258 (2001) 21.

[11] L. Weber, U. Egli, J. Mater. Sci. 12 (1977) 1981.

[12] S. Green, J. Backholm, P. Georén, C. G. Granqvist, G. A. Niklasson, Sol. Energy Mater. Sol. Cells 93 (2009) 2050.

[13] M. Mayer, SIMNRA: A simulation program for the analysis of NRA, RBS and ERDA, AIP Conf. Proc. 475 (1999) 541.

[14] MultiPak Software Release Notes Version 6.1A, Physical Electronics, Inc., Eden Prairie, MN, USA, 1999.

[15] A. Kuzmin, R. Kalendarev, A. Kursitis, J. Purans, J. Non-Cryst. Solids 353 (2007) 1840.

[16] F. de Groot, A. Kotani, Core Level Spectroscopy of Solids, CRC Press, Boca Raton, FL, USA, 2008.

[17] J. F. Moulder, W.F. Stickle, P.E. Sobol, Handbook of X-ray Photoelectron Spectroscopy, Physical Electronics Inc., MN, USA, 1995.

[18] J. Zhang, J. P. Tu, X. H. Xia, Y. Qiao, Y. Lu, Sol. Energy Mater. Sol. Cells 93 (2009) 1840.

[19] K. T. Ng, D. M. Hercules, J. Phys. Chem. 80 (1976) 2094.

[20] S. Uhlenbrock, C. Scharfschwerdt, M. Neumann, G. Illing, H.J. Freund, J. Phys.: Cond. Matter 4 (1992) 7973.

[21] A. P. Grosvenor, M. C. Biesinger, R. St. C. Smart, N. S. McIntyre, Surface Sci. 600 (2006) 1771.

[22] E. Avendaño, H. Rensmo, A. Azens, A. Sandell, G. de M. Azevedo, H. Siegbahn, G. A. Niklasson, C. G. Granqvist, J. Electrochem. Soc. 156 (2009) P132.

[23] G. van der Laan, J. Zaanen, G. A. Sawatzky, R. Karnatak, J. M. Esteva, Phys. Rev. B 33 (1986) 4253.

[24] J. van Elp, H. Eskes, P. Kuiper, G. A. Sawatzky, Phys. Rev. B 45 (1992) 1612.

[25] A. Fujimori, F. Minami, Phys. Rev. B 30 (1984) 957.

[26] M. N. Mancheva, R. S. Iordanova, D. G. Klissurski, G. T. Tyuliev, B. N. Kunev, J. Phys. Chem. 111 (2007) 1101.

[27] A. N. Mansour, C. A. Melendres, Surface Sci. Spectra 3 (1994) 2718.

[28] V. I. Nefedov, Y. V. Salyn, G. Leonhardt, R. Scheibe, J. Electron Spectrosc. Related Phenomena 10 (1977) 121.

[29] W. Lisowski, A. H. J van den Berg, G. A. M Kip, L. J. Hanekamp, Fresenius J. Anal. Chem. 341 (1991) 196.

[30] O. Yu. Khyzhun, J. Alloys Compounds 305 (2000) 1.

[31] Joint Committee on Powder Diffraction Standards - International Centre for Diffraction Data, card number: 83-0950

[32] Joint Committee on Powder Diffraction Standards - International Centre for Diffraction Data, card number: 15-0755

[33] Joint Committee on Powder Diffraction Standards - International Centre for Diffraction Data, card number: 78-0429

[34] J. V. Gabrusenoks, P. D. Cikmach, A. R. Lusis, J. J. Kleperis, G. M. Ramans, Solid State Ionics 14 (1984) 25.

[35] M. F. Daniel, B. Desbat, J. C. Lassegues, B. Gerand, M. Figlarz, J. Solid State Chem. 67 (1987) 235.

[36] S. H. Lee, H. M. Cheong, J. G. Zhang, A. Mascarenhas, D. K. Benson, S. K. Deb, Appl. Phys. Lett. 74 (1999) 242.

[37] E. Cazzanelli, A. Kuzmin, G. Mariotto, N. Mironova-Ulmane, J. Phys.: Cond. Matter 15 (2003) 2045.

[38] Y. Liu, H. Wang, G. Chen, Y. D. Zhou, B. Y. Gu, B. Q. Hu, J. Appl. Phys. 64 (1988) 4651.

[39]A. Kalinko, A. Kuzmin, J. Luminescence 129 (2009) 1144.

List of figure and table captions

Figure 1: Composition of Ni_xW_{1-x} oxide thin films as determined by two techniques *vs* ratio of sputter powers, and visual impression.

Figure 2: W 4f XPS spectra for pure W oxide and mixed Ni_xW_{1-x} oxide films. The small peak at 41 to 42 eV is due to W $5p_{3/2}$.

Figure 3: Ni $2p_{3/2}$ XPS spectra for mixed Ni_xW_{1-x} oxide films.

Figure 4: O 1s XPS spectra for pure W oxide and mixed Ni_xW_{1-x} oxide films.

Figure 5: XRD patterns for annealed films of $Ni_{0.5}W_{0.5}$ oxide (top) and pure W oxide (bottom). (*h k l*) parameters refer to the monoclinic phases of $NiWO_4$ and WO_3.

Figure 6: XRD patterns for an as-deposited film of NiO (top) and an annealed $Ni_{0.75}W_{0.25}$ oxide film (bottom). (*h k l*) parameters refer to the cubic rock-salt structure of NiO. Peaks marked by asterisks are tentatively attributed to $NiWO_4$.

Figure 7: Room temperature Raman spectra of pure W oxide and mixed Ni_xW_{1-x} oxide films with different magnitudes of *x*. Vertical lines indicate the positions of the two main bands at about 790 and 970 cm^{-1}.

Figure 8: Raman spectra for mixed Ni_xW_{1-x} oxide film with $x = 0.12$ (solid curve) and for a model (dots) corresponding to a weighted sum of two Raman signals: 76 % of pure W oxide and 24 % of $Ni_xW_{\mathbf{1-x}}$ oxide with $x = 0.45$.

Table 1: Summary of structural phases found in sputter deposited Ni_xW_{1-x} oxide films and of the experimental techniques used to obtain this information. XPS, RS and XRD denote X-ray photoelectron spectroscopy, Raman spectroscopy and X-ray diffractometry, respectively.

table 1

x in Ni_xW_{1-x} oxide	Phase	Experimental technique
$x < 0.50$	Amorphous WO_y	XPS (W 4f, O 1s), RS
	Nanosized $NiWO_4$	XPS (Ni 2p, O 1s), RS
$x = 0.50$	Nanosized $NiWO_4$	XPS (W 4f, Ni 2p), RS, XRD
	other	XPS (O 1s)
$x > 0.50$	NiO	XPS (O 1s, Ni 2p), XRD
	other	XPS (O 1s, Ni 2p)
	W^{5+} - phase	XPS (W 4f)
	Nanosized $NiWO_4$	XRD

figure 1
Click here to download Figures (if any): figure 1.EPS

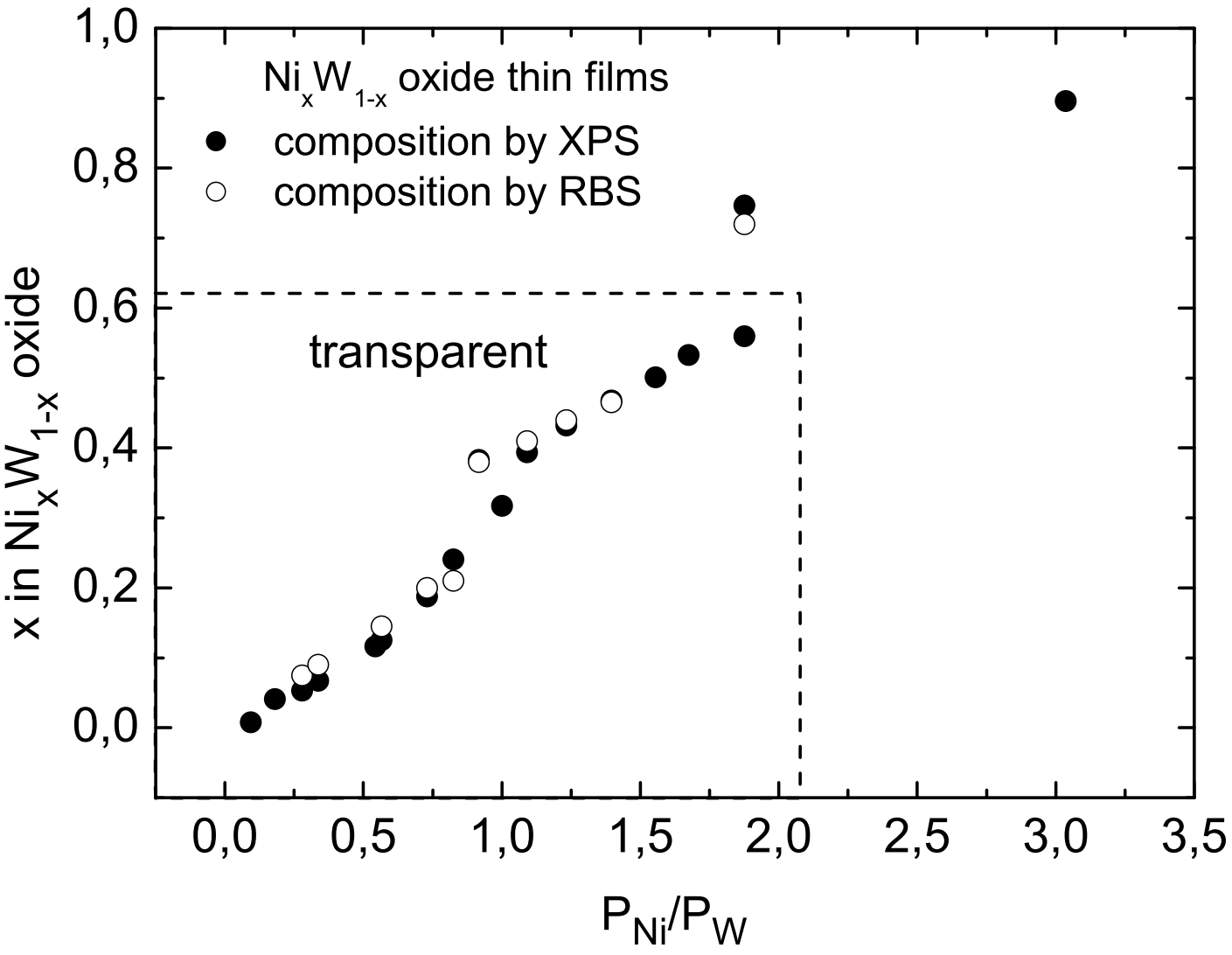

figure 2
Click here to download Figures (if any): figure 2.EPS

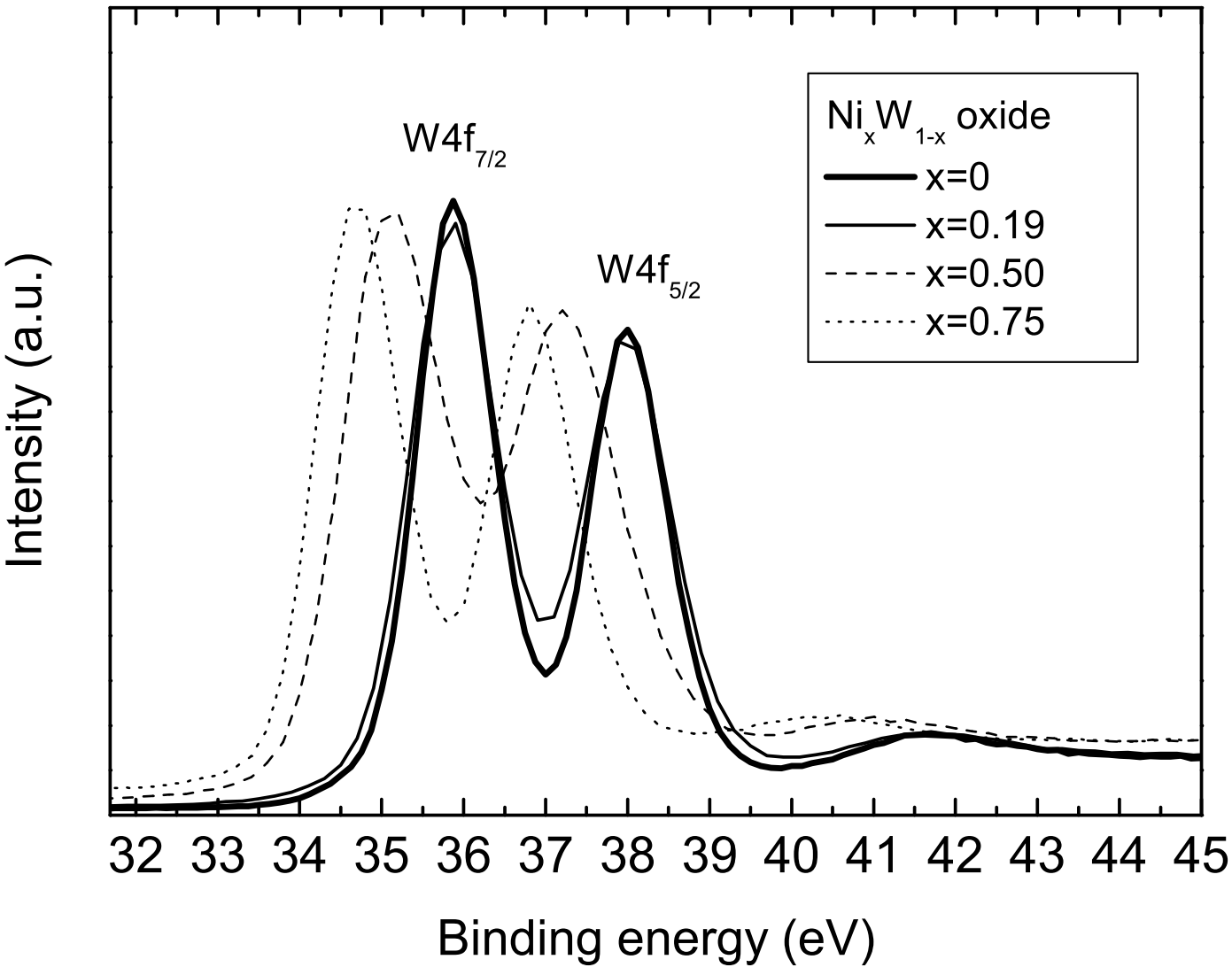

figure 3
Click here to download Figures (if any): figure 3.EPS

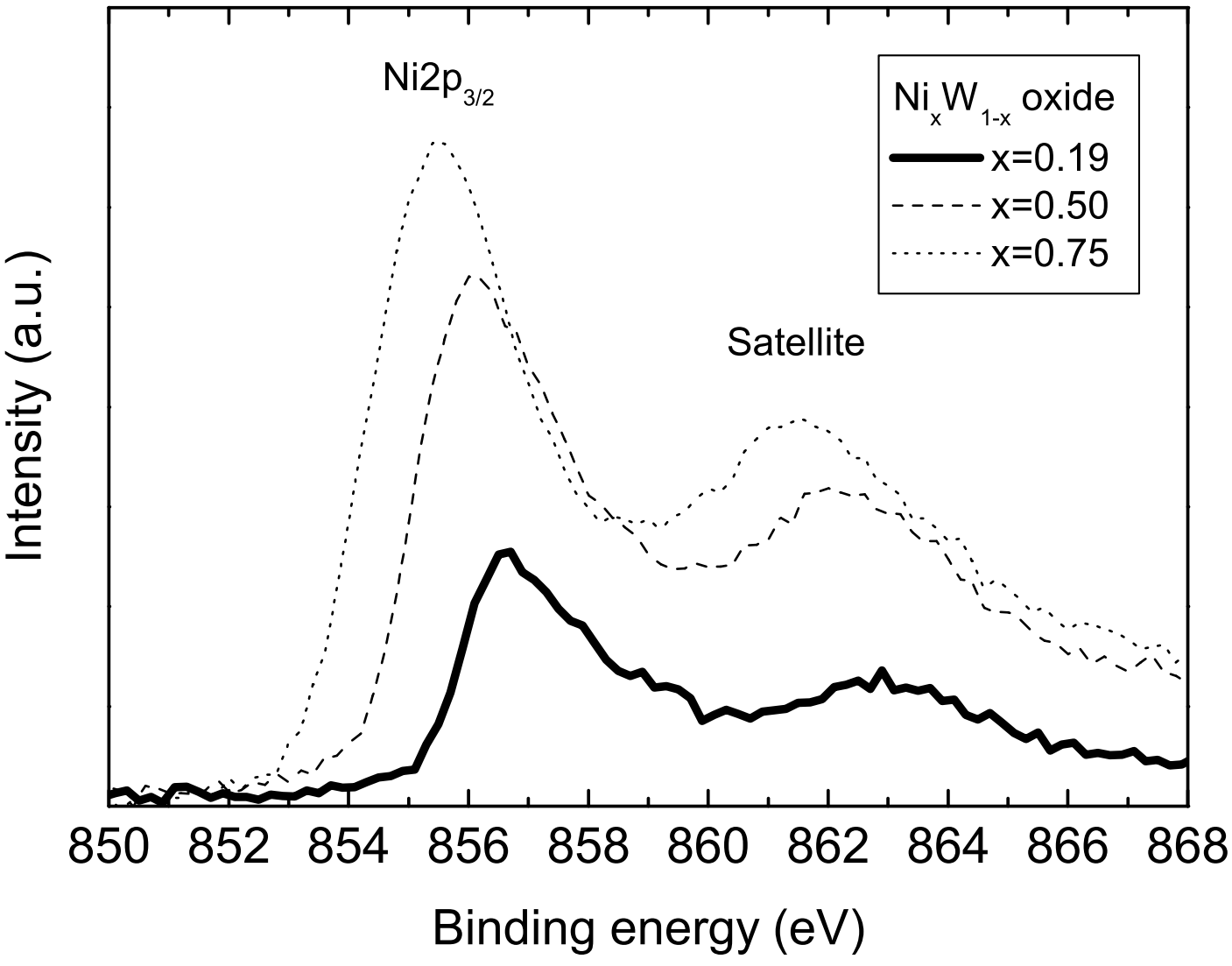

figure 4
Click here to download Figures (if any): figure 4.EPS

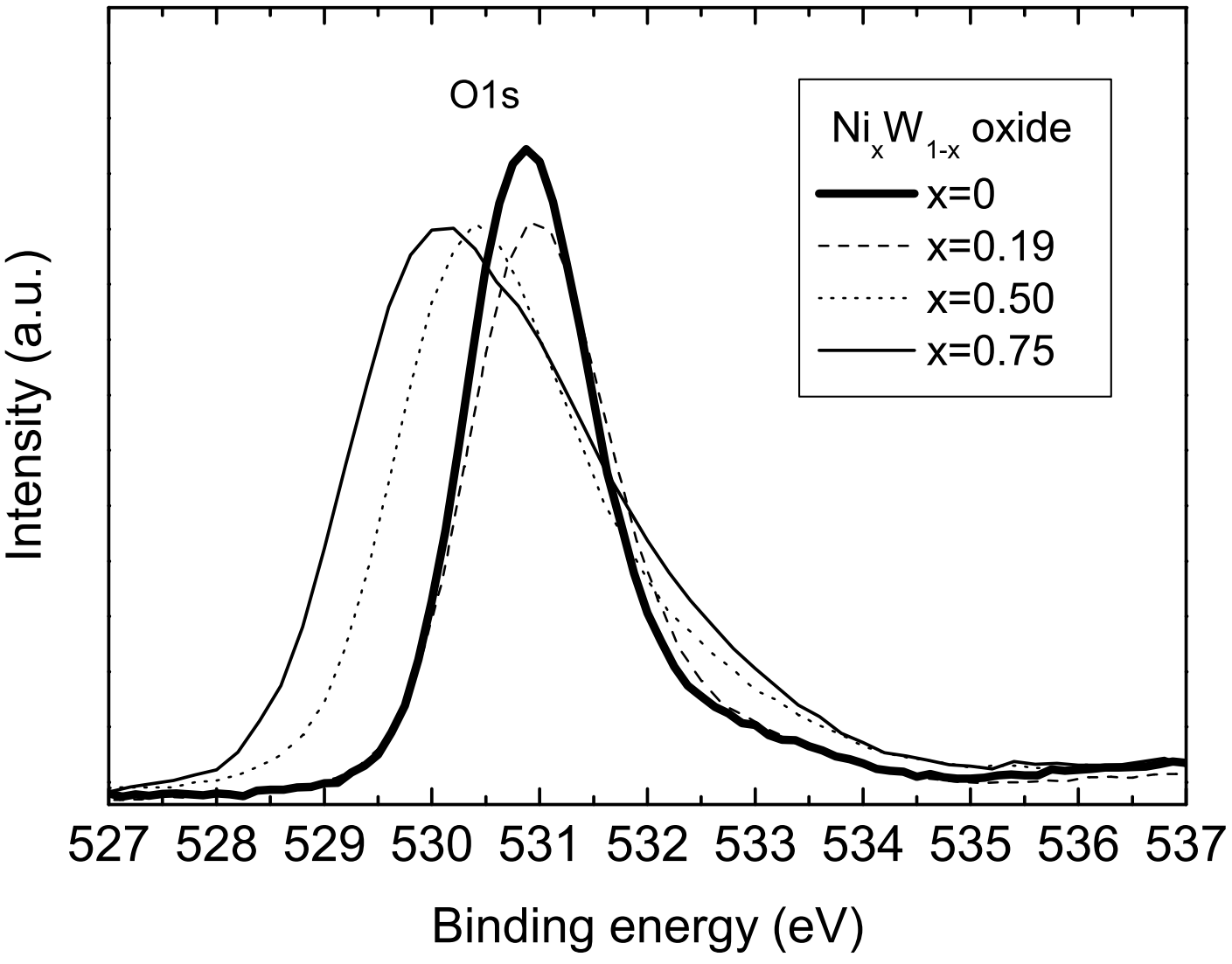

figure 5
Click here to download Figures (if any): figure 5.EPS

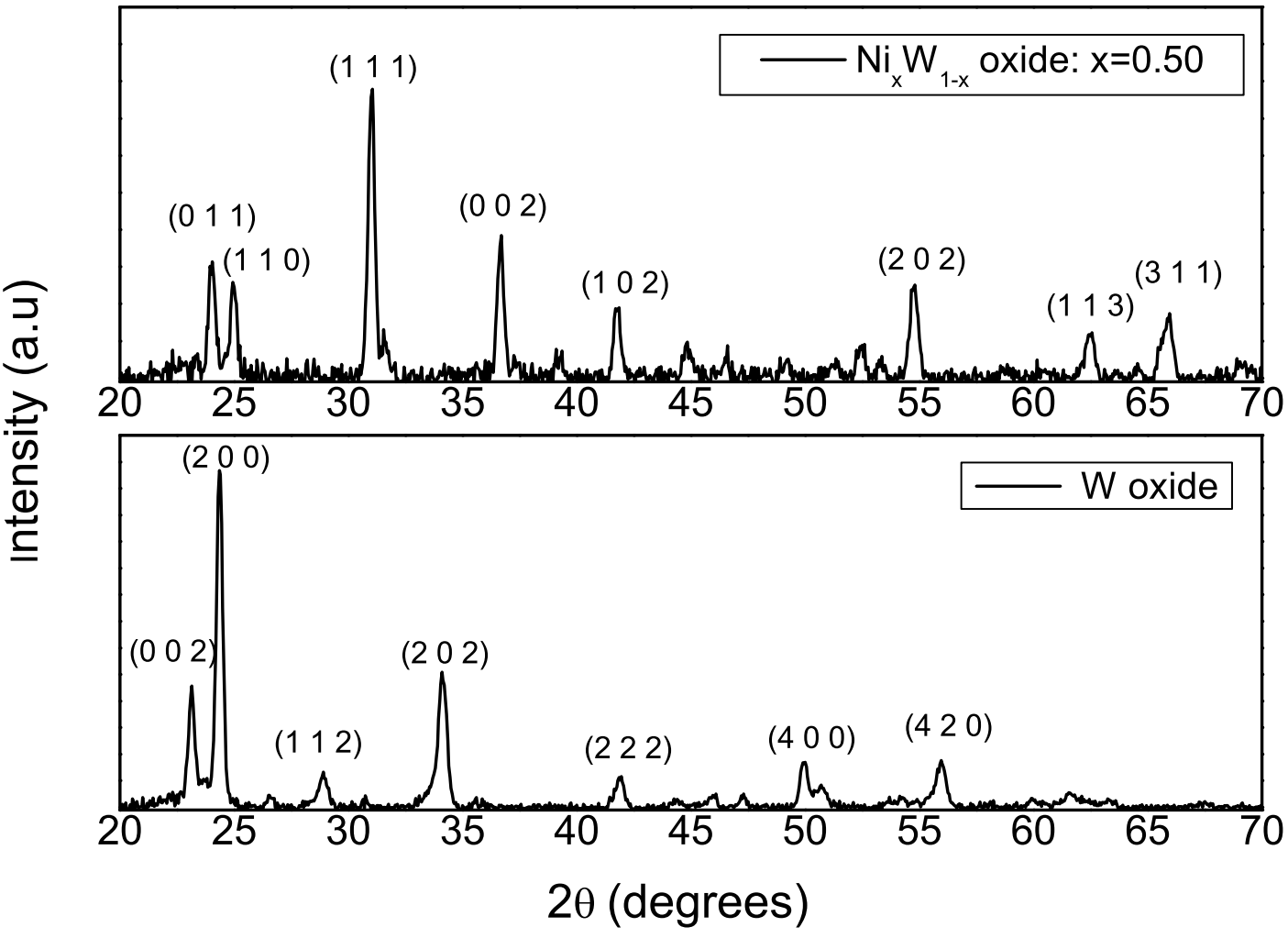

figure 6
Click here to download Figures (if any): figure 6.EPS

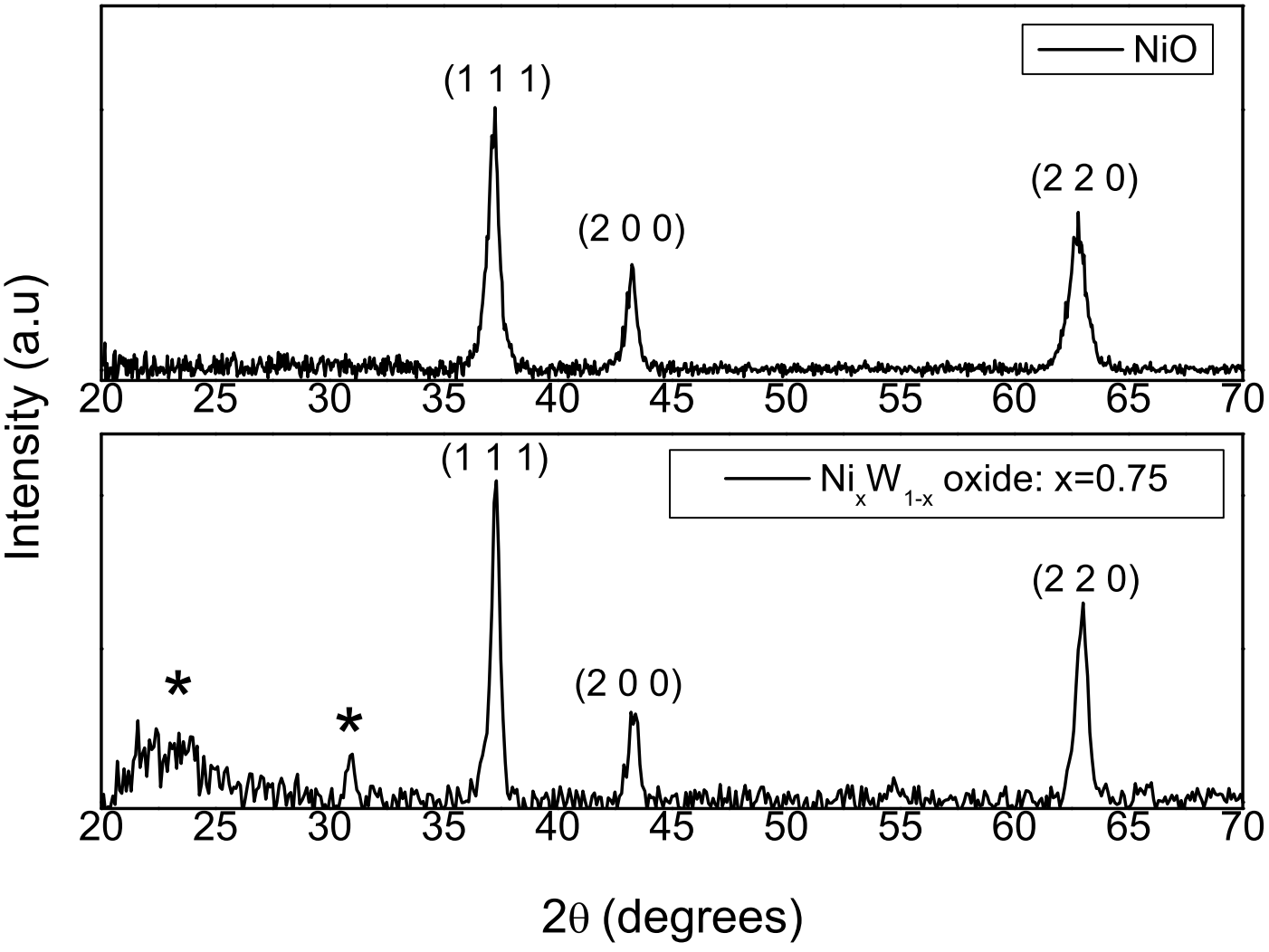

figure 7
Click here to download Figures (if any): figure 7.EPS

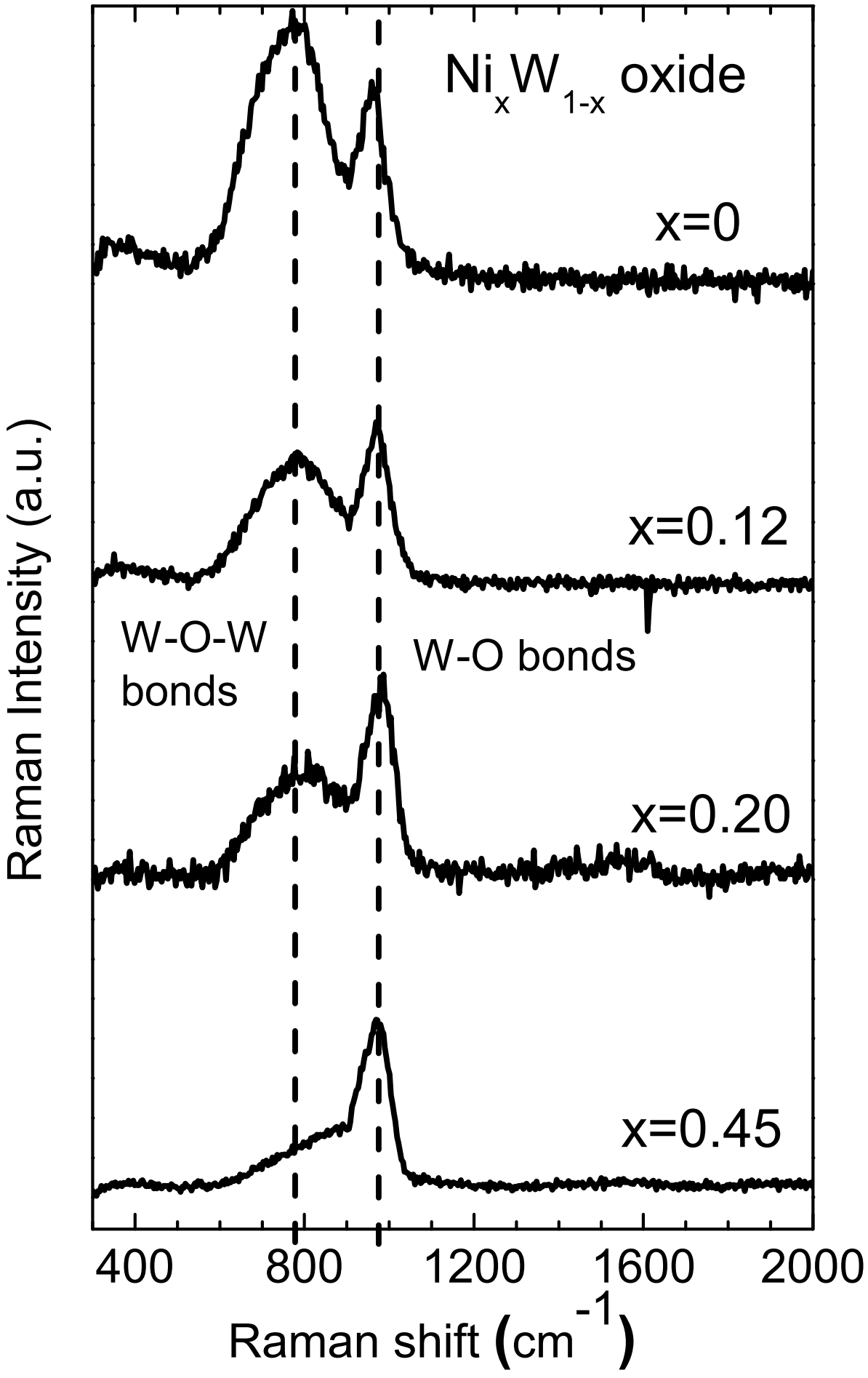

figure 8
Click here to download Figures (if any): figure 8.EPS